Deployment of Bistable Self-Deployable Tape Spring Booms Using a Gravity Offloading System

Huina Mao[1]; Pier Luigi Ganga, Ph.D.[2]; Michele Ghiozzi[3]; Nickolay Ivchenko, Ph.D.[4]; and Gunnar Tibert, Ph.D.[5]

Abstract: Bistable tape springs are suitable as deployable structures thanks to their high packaging ratio, self-deployment ability, low cost, light weight, and stiffness. A deployable booms assembly composed of four 1-m long bistable glass fiber tape springs was designed for the electromagnetically clean 3U CubeSat Small Explorer for Advanced Missions (SEAM). The aim of the present study was to investigate the deployment dynamics and reliability of the SEAM boom design after long-term stowage using onground experiments and simulations. A gravity offloading system (GOLS) was built and used for the onground deployment experiments. Two booms assemblies were produced and tested: a prototype and an engineering qualification model (EQM). The prototype assembly was deployed in a GOLS with small height, whereas the EQM was deployed in a GOLS with tall height to minimize the effects of the GOLS. A simple analytical model was developed to predict the deployment dynamics and to assess the effects of the GOLS and the combined effects of friction, viscoelastic relaxation, and other factors that act to decrease the deployment force. Experiments and simulations of the deployment dynamics indicate significant viscoelastic energy relaxation phenomena, which depend on the coiled radius and stowage time. In combination with friction effects, these viscoelastic effects decreased the deployment speed and the end-of-deployment shock vibrations. **DOI: 10.1061/(ASCE)AS.1943-5525.0000709.**

Author keywords: Tape spring; Bistable; Deployment boom; CubeSat; Viscoelastic effect; Energy relaxation.

Introduction

Small satellites, such as CubeSats, have been continually gaining interest due to their low launch cost, low profile to accomplish some high-level goals, and education missions in industry, military, and university applications (Heidt et al. 2000). Scientific CubeSat missions require deployable structures for sensors and passive attitude control. However, the limited volume requires highly compact deployment mechanisms to reduce stowed volume and power consumption. Deployable structures made from ultrathin composite materials are suitable thanks to their low cost, lightness, and stiffness (Murphey et al. 2015). Tape springs are ultrathin composites which can be folded elastically, and the stored energy can be released through a single kinematic path (Iqbal and Pellegrino 2000; Murphey et al. 2010). Existing structures, e.g., the motor-controlled AstroTube tape spring boom (scalable up to 2 m, mass less than 0.3 kg and, volume less than 1U ($0.1 \times 0.1 \times 0.1$ m^3) and the self-contained linear meter-class deployable (SIMPLE) boom, acted as inspiration for the boom assembly presented in this paper [Reveles et al. 2015; Murphey et al. 2010; Jeon and Murphey 2011; T. W. Murphey et al., "Deployable space boom using bistable tape spring mechanism," U.S. Patent No. 8, 770, 522 (2014); Mallol and Tibert 2013].

Controlled deployment booms are known to provide a predictable and stable deployment behavior. However, these structures need motors and control mechanisms to make sure the structure deploys steadily (Lichodziejewski et al. 2005; Tsuda et al. 2011; Reveles et al. 2015). Motors and control mechanisms inevitably increase the complexity, mass, and volume (Jeon and Murphey 2011). However, an uncontrolled deployment is prone to jamming and failure. Hence, a predictable self-deployable mechanism is required to reduce the volume, complexity, and cost. Bistable tape springs could self-deploy between two stable configurations: from the coiled initial-stable state to the final uncoiled lower energy state (Iqbal and Pellegrino 2000). The bistable tape springs deployment mechanism provides an opportunity to meet the requirements of small satellites (Jeon and Murphey 2011; Fernandez et al. 2011; Costantine et al. 2012; Footdale and Murphey 2014). As an example, the 1 m SIMPLE boom increases the capabilities of CubeSat missions thanks to the highly compact deployment mechanism with a stowed volume of $38 \times 38 \times 50$ mm^3 and a packaging length ratio lower than 4% (Murphey et al. 2010; Jeon and Murphey 2011). Other bistable tape spring structures are the 3.6 m long booms of a 5×5 m^2 solar sail (Fernandez et al. 2011). Footdale and Murphey (2011) designed and tested a CubeSat diffraction telescope with bistable tape springs, which can self-deploy from a 1U stowed configuration into an approximately 0.5-m tetrahedron (Footdale et al. 2013).

Thanks to the bistable nature the tape springs do not need to be restrained and only need to be guided by small rollers throughout deployment. However, the uncontrolled dynamics for self-deployed

[1]Ph.D. Student, Dept. of Aeronautical and Vehicle Engineering, KTH Royal Institute of Technology, Teknikringen 8, SE 100 44 Stockholm, Sweden. E-mail: huina@kth.se

[2]Structural Manager, Kayser Italia S.r.l., Via di Popogna, 501, 57124 Livorno, Italy. E-mail: p.ganga@kayser.it

[3]Mechanical Engineer, Kayser Italia S.r.l., Via di Popogna, 501, 57124 Livorno, Italy. E-mail: m.ghiozzi@kayser.it

[4]Associate Professor, Alfvén Laboratory, KTH Royal Institute of Technology, Teknikringen 31, SE 100 44 Stockholm, Sweden. E-mail: nickolay@kth.se

[5]Associate Professor, Dept. of Aeronautical and Vehicle Engineering, KTH Royal Institute of Technology, Teknikringen 8, SE 100 44 Stockholm, Sweden (corresponding author). E-mail: tibert@kth.se

Note. This manuscript was submitted on March 29, 2016; approved on September 21, 2016; published online on January 31, 2017. Discussion period open until June 30, 2017; separate discussions must be submitted for individual papers. This paper is part of the ***Journal of Aerospace Engineering***, © ASCE, ISSN 0893-1321.

structures can cause damage to the structure or to the spacecraft, so a good understanding and prediction of the self-deployment and the end-of-deployment shock vibration is required. A damper element may be used to control the deployment speed, but it could lead to extra mass, extra complexity, or an incomplete deployment. Some unforeseen anomalies might occur during the release of booms and lead to unexpected deployment because of variable thermal conditions. For example, the Mars Advanced Radar for Subsurface and Ionosphere Sounding (MARSIS) booms only partially deployed during self-deployment in space due to viscoelastic and thermal effects (Adams and Mobrem 2009).

A lot of research has been performed on both the quasi-static and dynamics behaviors of composite bistable tape springs (Iqbal and Pellegrino 2000; Mallikarachchi and Pellegrino 2014; Murphey et al. 2015), but the deployment dynamics has not been fully understood as various complex behaviors come into play, e.g., microbuckling mechanics, viscoelastic energy relaxation, and deployment latency. The end-of-deployment shock may cause damage to the structures and the deployment may also involve buckling and large rotations (Mallikarachchi 2011).

The viscoelastic effects cause a reduction in deployment moment or force for bistable composite tape springs and other folded composites after long periods of stowage (Adams and Mobrem 2009; Mobrem and Adams 2009; Kwok and Pellegrino 2010, 2011; Brinkmeyer et al. 2013; Murphey et al. 2015; Brinkmeyer et al. 2016). Viscoelastic effects in tape springs have been studied by experiments, numerical methods, and finite-element methods. Kwok and Pellegrino (2013) experimentally studied the bent folding, stowage, and deployment of tape springs. The folding and stowage process is characterized by significant energy relaxation; an energy reduction of as much as 60% is possible during stowage. Peterson and Murphey (2013) show through tests, modified micromechanics, and classical lamination theory analysis that the longitudinal and transversal bending stiffness of the tape spring decrease when the shear modulus decreases over time. Their test results are 10% less than predicted values due to inaccuracies in material property values and notable thickness. Brinkmeyer et al. (2013) experimentally show that the bistability of the structure always increases with viscoelastic strain energy relaxation and an initially bistable structure may not self-deploy from its coiled state due to this relaxation. Stowage of the structure at higher temperature or for longer periods of time increases the deployment time. The relaxation may be beneficial in reducing dynamic effects of a rapid deployment and reduce the risk of material failure (Brinkmeyer et al. 2016). However, the structure might also fail to deploy and become stable at any extended length at higher temperature, i.e., the structure has transitioned from being bistable to neutral stable for stowage 3 h at 100°C, where the tape springs have the same strain energy in the fully coiled and extended states (Brinkmeyer et al. 2013; Murphey and Pellegrino 2004). A model to predict the deployment dynamics of single tape springs was developed by Brinkmeyer et al. (2013), and one finding was that the deployment dynamics are difficult to model for relaxation during stowage. Finite-element simulations based on linear viscoelastic material models have been used to capture the viscoelastic effects in stowage and deployment of bent tape springs, and modeling results were very sensitive to the micromechanics of the uneven thickness distribution (Kwok and Pellegrino 2011; Kwok and Pellegrino 2013). Mallol (2013) used the finite-element method to model a 1 m fully coiled bistable boom based on the SIMPLE boom design. Compared with the experiments the finite-element simulation predicted a deployment that was six times faster. One possible reason of the discrepancies between simulations and experiments is that at high strains the matrix material is not linear elastic but exhibits viscoelastic behaviors (Mallol 2013; Brinkmeyer et al. 2016). Another possible reason is that the deployment speed of bistable tape springs also depends on friction and contact, which are very difficult to model accurately in finite-element models. Solutions to the viscoelastic energy relaxation have been found through micromechanical approaches (Kwok and Pellegrino 2011, 2012, 2013). Kwok and Pellegrino (2012) presented a micromechanical finite-element model and studied the deployment and recovery of a bent thin-walled viscoelastic tape spring with close agreement to experimental results. However, micromechanical models are difficult to implement in the deployment simulation of a complete boom system and are computationally expensive. Therefore, an analytical model that includes nonlinear viscoelastic effects and friction in a simple way is needed for further experimental and computational studies of complete tape spring booms. The goal of the present study is to investigate the deployment dynamics and reliability of the SEAM boom design after long-term stowage using onground experiments and simulations.

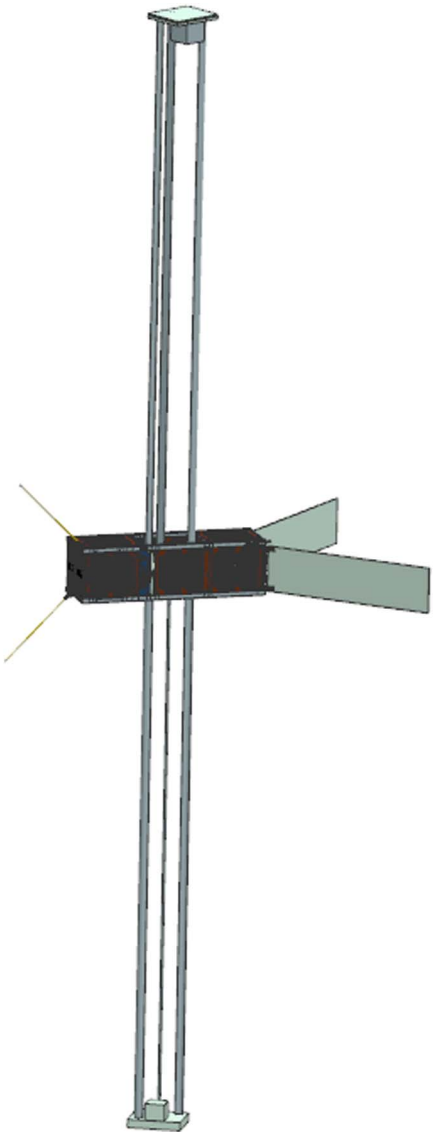

Fig. 1. Concept view of the 3U SEAM CubeSat (image by Gunnar Tibert)

Bistable tape spring booms will be used for the 3U CubeSat Small Explorer for Advanced Missions (SEAM). The SEAM project will put a CubeSat in a 600-km altitude sun-synchronous

orbit with a one year lifetime (Fig. 1) (Ivchenko 2012). The goals of the SEAM project are to develop and demonstrate for the first time an electromagnetically clean nanosatellite with precision attitude determination, flexible autonomous data acquisition system, wideband telemetry, and integrated solution for ground control and data handling. The primary payloads of SEAM are the magnetic and electric fields sensors. SEAM is led by KTH (Royal Institute of Technology) in cooperation with a consortium of companies: ÅAC Microtec, ECM office, Laboratory for Electromagnetic Innovations (LEMI), BL-Electronics, GomSpace, Swedish Space Corporation (SSC) and Kayser Italia. Since interferences produced by the satellite should be negligible compared with the Earth's electromagnetic field, two 1-m long tape spring booms based on the SIMPLE boom design [Murphey et al. 2010; Jeon and Murphey 2011; T. W. Murphey et al., "Deployable space boom using bistable tape spring mechanism," U.S. Patent No. 8, 770, 522 (2014)], were selected to place the sensors away from the CubeSat for accurate measurements. As the bistable tape spring booms might be kept stowed for several months before deployment the energy relaxation effects must be considered and mitigated in design. A finite-element analysis is too complex and not sufficiently accurate to catch the true deployment dynamics including friction and energy relaxation (Mallol 2013; Mallol and Tibert 2013). A simple and robust simulation model is required to predict the deployment of the SEAM booms and other similar booms. Ground experiment must be performed to validate the analytical model and to quantify the friction and the energy relaxation effect on the deployment dynamics.

The remainder of the paper is outlined as follows. In section "Deployment System Design and Gravity Offloading System" an overview of the SEAM boom design and the gravity offloading system (GOLS) are presented. In section "Predicting the Deployment of Tape Spring Booms" an analytical model is proposed to predict the deployment dynamics of the tape spring booms. In section "Onground Deployment Experiments" the ground deployment tests of a prototype of the booms assembly in an initial GOLS and of an engineering qualification model (EQM) of the booms assembly in an improved GOLS are presented and analyzed. In section "Discussion" the theoretical deployment force is calculated and compared with the experiment results, and section "Conclusion" consists of the presentation of the conclusion of the experiments and simulations.

Deployment System Design and Gravity Offloading System

Bistable Tape Spring Booms and Deployment System Design

Bistable tape springs are typically made from high-strength glass fibers or carbon fibers (Herlem 2014; Murphey et al. 2015). Previous experience with tape springs made from woven carbon fibers suggested that tape springs made from glass fibers would provide a good design considering material availability, stored strain energy, and deployed stiffness (Mallol 2013; Mallol and Tibert 2013). In order to have enough deployment energy, i.e., to overcome the matrix energy relaxation, the bistable tape springs were fabricated from four layers of preimpregnated Hexply $M77W/38\%/107P/G$ fabric and the lay directions are $[-45F/0F/90F/+45F]$, where $0F$ represents the fabric layer in longitudinal direction (Herlem 2014; Ekelöw 2014). Hexply $M77W/38\%/107P/G$ is an epoxy E-glass plain weave prepreg, whereby $M77W$ is the resin type, 38% is the resin content by weight, and the nominal area weight is 107 g/m^2 with 53 g/m^2 fibers in 0° direction and 51 g/m^2 fibers in 90° direction (Hexcel Corporation 2014; Hexcel Corporation 2013). The thickness of each layer is 0.097 mm. The midradius, R, and angle, β, of the cross section circular arc of the 1-m long tape springs are 7.2 mm and 180°, respectively. Material properties were measured by an Instron 5,567 Series machine and three-dimensional (3D) digital image correlation system. The tensile modulus in 0° and 90° directions were $E_1 = 20$ GPa and $E_2 = 19.5$ GPa, respectively. The Poisson's ratio $\nu_{12} = 0.11$ and the shear modulus $G_{12} = 3.5$ GPa. Tape spring bistability is given by the outer ±45° layers, but as the viscoelastic energy relaxation is attributed to shear strain in the outer ±45° layers (Peterson and Murphey 2013) two inner layers 0°/90° are used to mitigate the relaxation effects and increase the deployment force. The laminate was cured at 125°C for 2 h. The tape spring was placed in a vacuum bag with full vacuum (approximately 0 Pa), and the vacuum pump was kept on during the curing process to ensure a smooth outer surface of the tape springs.

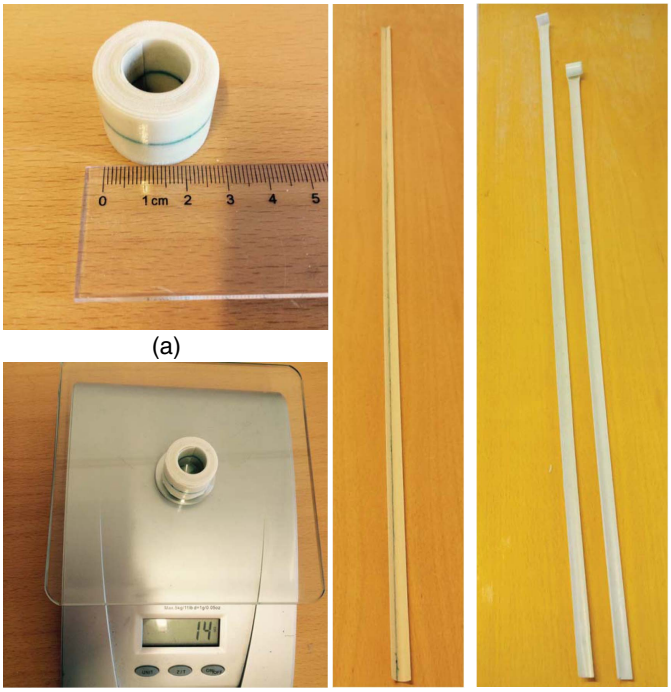

Fig. 2. 1 m glass fiber bistable tape springs: (a) coiled stable state; (b) mass of one tape spring; (c) extended stable state; (d) partially deployed tape springs (image by Huina Mao)

Thus, through the four-layer-layup the tape springs were designed to mitigate viscoelastic relaxation effects so that the end masses of the boom could be deployed (even after long-term stowage). The bistability criterion indicated that the designed tape springs would not be bistable immediately after fabrication if friction, viscoelastic relaxation, hysteresis, and manufacturing errors were neglected (Guest and Pellegrino 2006). However, 12 of the 16 tape springs were bistable immediately after fabrication, while four became bistable after being coiled for a few hours. It was observed that the SEAM tape springs (Fig. 2) are straighter compared to the tape spring in Brinkmeyer et al. (2016) that twists approximately 140 degree/m after demolding. One reason is that the plain-weave fabric has approximately the same amount of fibers both in longitudinal and transversal directions compared with the unidirectional fabric in Brinkmeyer et al. (2016), so the laminate is nearly balanced and symmetric and the bending-stretching coupling is nearly zero. This allows fabrication of twist-free tape springs, which are resistant to thermally induced cross section deformations

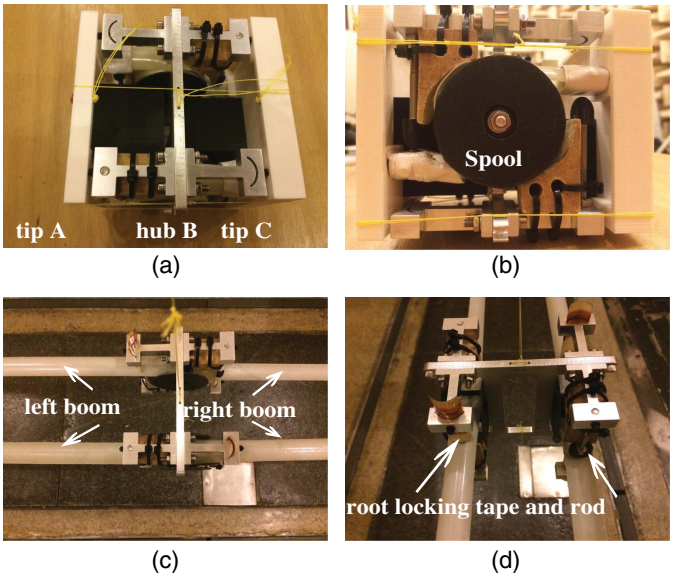

Fig. 3. Prototype of the self-deployable SEAM booms assembly (image by Huina Mao)

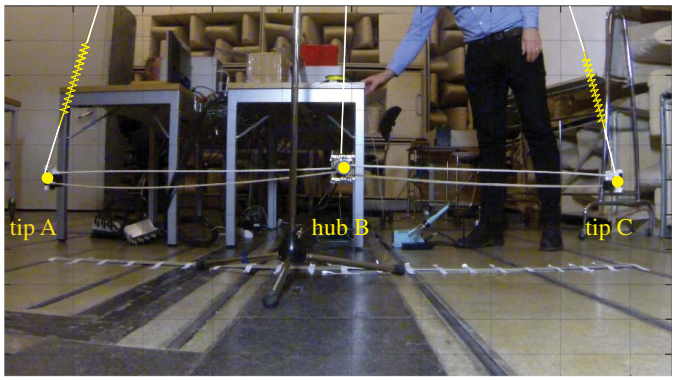

Fig. 4. Fully deployed booms assembly suspended in a GOLS (image by Huina Mao)

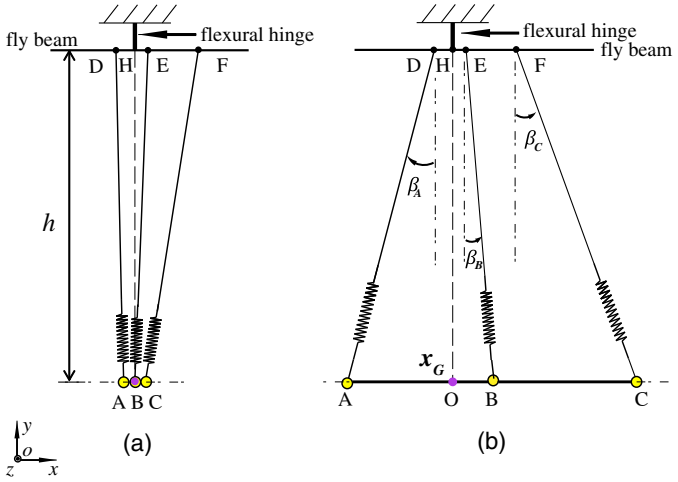

Fig. 5. Two GOLS with different equilibrium states (not to scale): (a) initial equilibrium state: the booms are fully coiled in the stowed configuration; (b) final equilibrium state: the booms are fully extended

(Peterson and Murphey 2013). The natural coiling radius of the tape springs was 12.5 mm, and they are bistable with a coiling radius between 10 and 15.5 mm [Fig. 2(a)]. The lightweight tape spring, which is approximately 14 g/m [Fig. 2(b)], self-deployed from the coiled to the extended stable state [Fig. 2(c)]. After being stowed for 10 months at room temperature and with an initial coiling radius of 10 mm, the tape springs self-deployed to more than 90% of the length [Fig. 2(d)]. All tape springs in the present study were stored at room temperature with an inner coiling radius of 10 mm. The details of the manufacturing of the tape springs are described in Herlem (2014) and Ekelöw (2014).

Fig. 3 shows a prototype of the stowed SEAM booms assembly based on the patented SIMPLE boom [Murphey et al. 2010; T. W. Murphey et al., "Deployable space boom using bi-stable tape spring mechanism," U.S. Patent No. 8, 770, 522 (2014)]. The booms were composed of four 1-m bistable tape springs that were elastically coiled on two counter rotating spools and stowed in the central hub, $m_B = 0.230$ kg, with a volume of $100 \times 80 \times 95$ mm^3. Tip masses ($m_A = 0.240$ kg and $m_C = 0.255$ kg) were fixed on the left and right tip of the booms and deployed simultaneously through the kinematic coupling [Fig. 3(a)]. A 0.39-mm diameter ultrahigh-molecular-weight (UHMW) polyethylene-braided cord was circled around the prototype booms assembly to prevent self-deployment. When the cord was cut the strain energy was released to deploy the end masses. Root-locking tapes and rods [Fig. 3(d)] were used to guide the tape springs during deployment and to make the root of the booms stiffer in bending and torsion.

Gravity Offloading System

A GOLS based on the Marionette Paradigm (Greschik and Belvin 2007) was adopted to simulate the zero gravity found in space. Fig. 4 shows the fully deployed booms assembly suspended in the GOLS, and Fig. 5 shows a schematic picture of the GOLS. The booms were hanging in a fly beam with braided cords and extension springs. The fly beam is a beam which is connected to the roof by a short-braided cord as a hinge. The stretch elasticity of the braided cord was very low and could be safely neglected. Soft extension springs were used to compensate for the changes in distance between the hanging points, tip masses, and the hub during deployment.

Different initial static equilibrium states and distances between hanging points (Fig. 5) were considered in order to minimize the effect of GOLS. The equilibrium state is a static equilibrium state when the vertical component of the extension spring force equals the weight of the supported object. Fig. 5 shows two static equilibrium states: the initial equilibrium state where the system was in static equilibrium when the booms were fully coiled in the initial stowed configuration, and the final equilibrium state where the system was in static equilibrium when the booms were fully extended.

If the braided cords were fixed in different points on the fly beam [Fig. 5(b)], a small out-of-xy-plane disturbance would lead to large and unexpected out-of-plane motion. If the hanging points were movable in the x-direction the friction between the fly beam and the hanging points would delay the deployment. Therefore, a single hanging point was selected for the authors' experiments, i.e., $x_D = x_H = x_E = x_F = 0$. As it was difficult to control the strained length of the extension springs to ensure full offloading of the end masses in the stowed configuration, the deployed configuration was used as the initial offloading configuration for the single-point GOLS of the prototype booms assembly, Fig. 6(a).

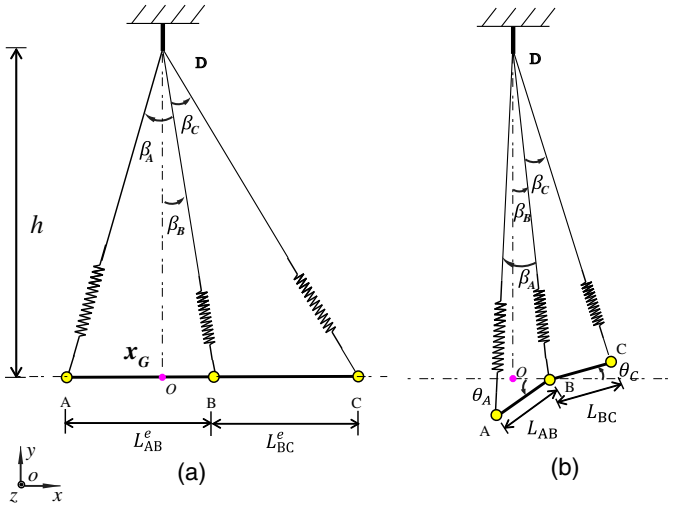

Fig. 6. Simplified model of the single-hanging point GOLS (not to scale): (a) final equilibrium state with fully extended; (b) configuration during deployment

Predicting the Deployment of Tape Spring Booms

Previous experience suggests that it is too complex to capture the deployment dynamics of complete boom systems with finite-element simulations as some effects (e.g., friction and viscoelastic effects) cannot be included accurately (Mallol 2013; Mallol and Tibert 2013). A simple two-dimensional (2D) analytical model allows a flexible implementation of various hard-to-capture effects at the system level rather than at a local detailed level.

It was assumed in Fig. 6 that h is much greater than the length of the booms, and the extension springs and braided cords were very light. The conservation of momentum gives that the center of gravity of the system in x-direction will not change during deployment

$$\sum_{i=1}^{3} m_i x_i = x_G \sum_{i=1}^{3} m_i \tag{1}$$

In the final equilibrium state [Fig. 6(a)] the equilibrium length $L^e_{AB} = L^e_{BC} = L^e_{AC}/2 = 1$ m, where L^e_{AC} is the fully deployed length of the whole booms assembly. Assuming $x_G = 0$ and that the momentum is conserved, the equilibrium position in Eq. (1) becomes

$$x^e_A = -(L^e_{AC} m_B + 2L^e_{AC} m_C)/(2m_A + 2m_B + 2m_C) \tag{2a}$$

$$x^e_B = L^e_{AC}/2 + x^e_A \tag{2b}$$

$$x^e_C = L^e_{AC} + x^e_A \tag{2c}$$

$$y^e_A = y^e_C = y^e_B = 0 \tag{2d}$$

The forces of the extension springs or braided cords in the final equilibrium position (F^e_{Di} and F^e_{DB}) are

$$F^e_{Di} \cos(\beta^e_i + \beta^e_B) = m_i g \tag{3a}$$

$$F^e_{DB} \cos(\beta^e_B) = m_B g \tag{3b}$$

where $i = A, C$; and the angles between the braided cords and the vertical axis are

$$\beta_B = \arctan(x_B/h) \tag{4a}$$

$$\beta_i = \arctan[x_i/(h - y_i)] - \beta_B \tag{4b}$$

Two soft extension springs were used for the tip masses, but no extension spring was used for the hub as the displacement of the hub, x_B, was very small when tip masses $m_A \approx m_C$. If the low-stretch UHMW braided cords are treated as infinitely stiff springs, the forces in the extension springs or braided cords during the deployment are

$$F_{Di} = k_{Di}(L_{Di} - L^0_{Di}) + F^{\min}_{Di} \tag{5a}$$

$$F_{DB} = m_B g/\cos\beta_B \tag{5b}$$

$$L_{Di} = \sqrt{(x_i - x_D)^2 + (y_i - y_D)^2} \tag{5c}$$

where $k_{Di} = 7$ N/m, $F^{\min}_{Di} = 0.7$ N, and L^0_{Di} are the spring stiffness, minimum extension force, and the free length of the soft extension springs, respectively.

Inserting the equilibrium positions [Eq. (2)] and spring forces [Eq. (3)] into Eq. (5), the free length of each spring, L^0_{Di}, is calculated. Then, the extension spring force only depends on the position of the suspended object during deployment [Eq. (5)].

Deployment Dynamics of Tape Spring Booms

The tip masses were deployed by the stored strain energy of the tape springs but decelerated by friction, the GOLS, and nonuniform viscoelastic energy relaxation due to long-term stowage. The deployment force acting on the tip masses in the x-direction is

$$F^x_i = F^x_{Bi} - F^x_{Di} \tag{6}$$

with

$$F^x_i = m_i \ddot{x}_i \tag{7a}$$

$$F^x_{Bi} = F_{Bi} \cos\theta_i \tag{7b}$$

$$F^x_{Di} = F_{Di} \sin(\beta_i + \beta_B) \tag{7c}$$

where F_{Bi} = deployment force from the tape springs on the tip mass (including friction and viscoelastic energy relaxation); θ_i = rotational angle of each boom in counter clockwise direction as shown in Fig. 6(b); and

$$\theta_i = \arctan\left(\frac{y_i - y_B}{x_i - x_B}\right) \tag{8}$$

Since the two booms deploy simultaneously, $L_{AB} = L_{BC}$, then

$$\frac{x_B - x_A}{\cos\theta_A} = \frac{x_C - x_B}{\cos\theta_C} \tag{9}$$

Assuming that θ_i is very small, $\dot{\theta}_A \approx \dot{\theta}_C$ and $\ddot{\theta}_A \approx \ddot{\theta}_C$, then

$$\frac{\ddot{x}_B - \ddot{x}_A}{\cos\theta_A} = \frac{\ddot{x}_C - \ddot{x}_B}{\cos\theta_C} \tag{10}$$

Since both tips had approximately equal masses, the movement of the hub and the rotation of tip masses (x_B, β_B, θ_i) are small, and the extension spring forces are assumed to be $F_{DA} = F_{DC}$.

Inserting Eq. (10) into Eqs. (6) and (7), the relationship between F_{BA} and F_{BC} can be derived as

$$F_{BA} = KF_{BC} \tag{11}$$

where

$$K = -\frac{m_A}{m_C}\left[\frac{m_C\cos\theta_C + \cos\theta_A(m_B + m_C)}{m_A\cos\theta_A + \cos\theta_C(m_A + m_B)}\right]\frac{\cos\theta_A}{\cos\theta_C}. \tag{12}$$

The deployment force F_{BC} is calculated from deployment experiments with the GOLS through the positions of the hub and tip masses [Eq. (13)]. The deployment force F_{BA} in simulation is calculated as the function of F_{BC} [Eq. (11)]. Thus, the deployment could be simulated according to the equations of motion: Eq. (13) when $|\theta_i| \le \theta_i^{\max}$ and Eq. (14) when $|\theta_i| > \theta_i^{\max}$, where $\theta_i^{\max}$ is the maximum rotational angle of each boom reached in deployment under the root-locking tapes and rods [Fig. 3(d)], and d_i (with unit J/s) is the damping factor of the boom in y direction which was computed from experimental results when $|\theta_i| = \theta_i^{\max}$

$$m_i\ddot{x}_i = F_{Bi}\cos\theta_i - F_{Di}\sin(\beta_B + \beta_i) \tag{13a}$$

$$\begin{aligned} m_i\ddot{y}_i = &-\text{sign}(x_i - x_B)F_{Bi}\sin\theta_i \\ &- F_{Di}\cos(\beta_B + \beta_i) - m_i g - d_i\dot{L}_{Bi} \end{aligned} \tag{13b}$$

$$m_i\ddot{x}_i = F_{Bi}\cos\theta_i - F_{Di}\sin(\beta_B + \beta_i) \tag{14a}$$

$$\dot{y}_i = \tan[\text{sign}(\theta_i)\theta_i^{\max}](\dot{x}_i - \dot{x}_B) + \dot{y}_B \tag{14b}$$

End-of-Deployment Shock Forces

After each tape spring is fully deployed into a semicircular cross-section the boom acts as a stiff spring

$$k_{Bi} = \eta_i E_{Bi}A_{Bi}/L_{Bi}^f \quad (L_{Bi}^f - r < L_{Bi} < L_{Bi}^f + r) \tag{15a}$$

$$k_{Bi} = E_{Bi}A_{Bi}/L_{Bi}^f \quad (L_{Bi} \ge L_{Bi}^f \pm r) \tag{15b}$$

where the radius of the spool $r = 0.01$ m; the fully deployed length $L_{Bi}^f = 1$ m; the elastic modulus $E_{Bi} \approx 17$ GPa calculated from the classical laminate theory; and the cross section area of the boom $A_{Bi} = 8.5$ mm^2. The softening factor of the stiff boom η_i (computed from experiments) is due to the small forward rotation of spools after full deployment. As Fig. 7 shows that the tape springs are softer between $L_{Bi}^f - r < L_{Bi} < L_{Bi}^f + r$ [Figs. 7(a and b) or 7(c and d)] than when $L_{Bi} \ge L_{Bi}^f \pm r$ [Figs. 7(b and c)] because the spools could rotate within $\pm 90°$ after full deployment, which needs less force for rotating the spools than for extension of a tape spring. The forces of each boom after full deployment is

$$F_{Bi}^{\text{post}} = k_{Bi}(L_{Bi} - L_{Bi}^f) \tag{16}$$

Thus, the end-of-deployment shock can be simulated from Eqs. (13) and (14) if F_{Bi} is replaced by F_{Bi}^{post}.

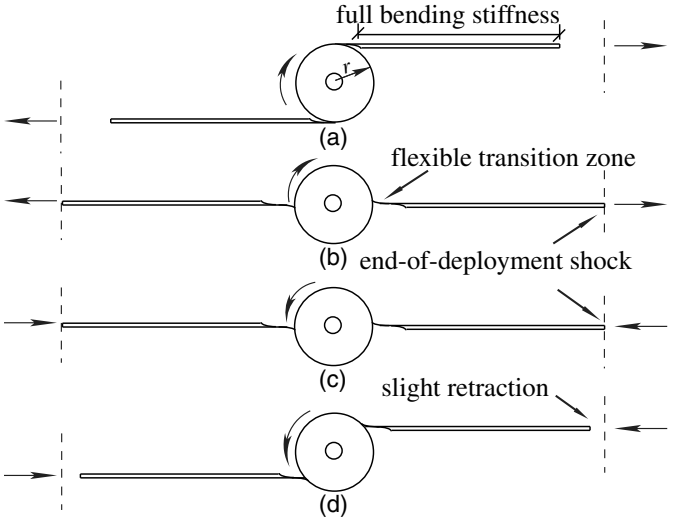

Fig. 7. After full deployment, the boom is in axial vibration (not to scale): lower axial stiffness from (a) to (b) and from (c) to (d); full axial stiffness from (b) to (c)

Onground Deployment Experiments

Experiment 1: Deployment of the Prototype Booms Assembly

The prototype model was deployed when suspended from a single-hanging point GOLS with a height $h = 4.17$ m, and the deployed length was recorded and extracted from images using a high resolution (1080p) camera with a frame rate of 60 frames per second (fps) (Fig. 8). The camera view was parallel to the deployment plane and visual distortion was calculated and corrected by the marked positions of a two-meter ruler along the deployed boom. The measurement uncertainty was approximately ± 2 mm. Before deployment the booms assembly had been stowed for four months at room temperature. When the constraining braided cord around the assembly was cut the booms started to deploy simultaneously and were fully deployed in 0.8 s. In contrast to the finite-element simulations of the SIMPLE boom design (Mallol 2013; Mallol and Tibert 2013), buckling of the tape springs and large rotations were not observed in the experiment. Small horizontal angles θ_i were observed during the deployment since the extension springs became shorter from the fully deployed equilibrium state [Fig. 6(a)] to the coiled state [Fig. 8 ($t = 0$ s)]. Thus, the extension springs could not fully offload the end masses, i.e., the end masses sunk until the booms were fully deployed, generating nonzero angles θ_i. Therefore, a higher ceiling and stiffer extension springs were desired to decrease the vertical movement and end-of-deployment oscillation of the end masses.

Fig. 9 shows the position of tip masses measured from images where the initial length of the booms $L_{Bi}^0 = 50$ mm [Fig. 3(b)]. The hub moved a little to the left during deployment because the left tip mass m_A was slightly smaller than the right tip mass m_C; x_A and x_B were slightly smaller than -1 and 1 m, respectively, for the same reason. The tip angles θ_A and θ_C were constrained to approximately $\theta_i^{\max} \approx 10°$; θ_A and θ_C were different between the tape springs because of the manually adjusted root locking tapes, Fig. 3(d).

The acceleration in x-direction of the hub was recorded by an accelerometer (Fig. 10). Since the accelerometer mass is only 5 g and placed on the hub (which moved only a very small distance during deployment), its influence on the deployment dynamics was

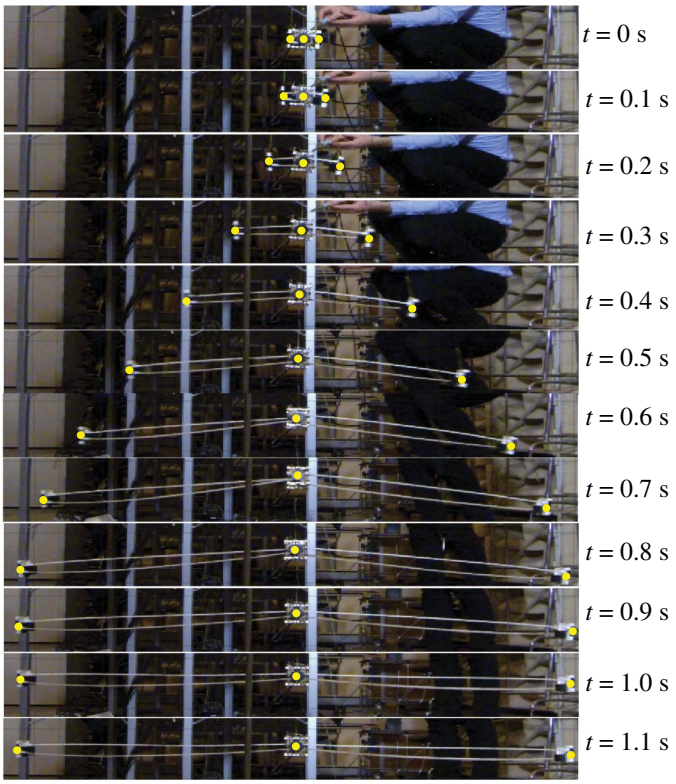

Fig. 8. Snapshots at $0, 0.1, 0.2, \ldots, 1.1$ s of the deployment sequence of Experiment 1 (image by Huina Mao)

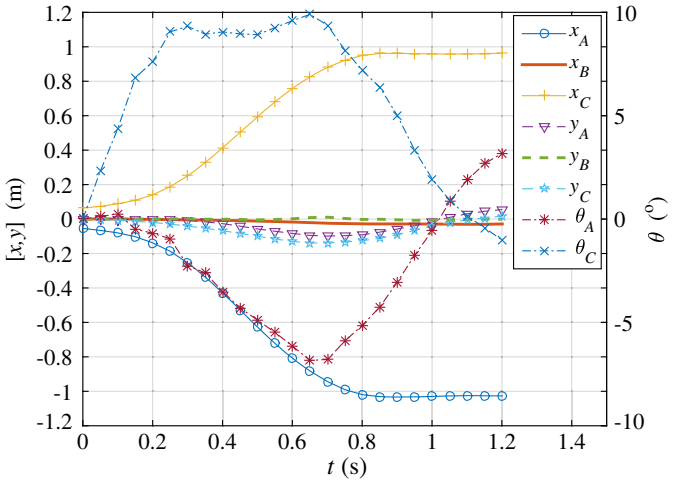

Fig. 9. Displacements and angles of tip masses and the hub of the booms deployment during Experiment 1

judged to be very small and was neglected. The maximum acceleration due to the end-of-deployment shock was observed when the boom was fully deployed at $t = 0.8$ s; it was less than 15 g (147 m/s^2). The vibration was almost fully damped out within 0.4 s after full deployment.

Result Analysis of Experiment 1

From the displacements of tip masses and the hub in Fig. 9, parameters $\ddot{x}_i$, β_i, F_{Di}, F_i, F_{Bi}, and K were derived from Eqs. (4)–(13).

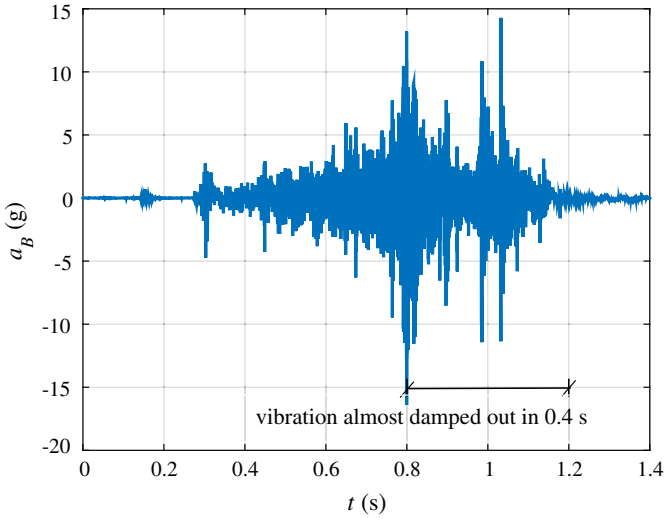

Fig. 10. Acceleration of the hub (mass B) in x-direction during Experiment 1

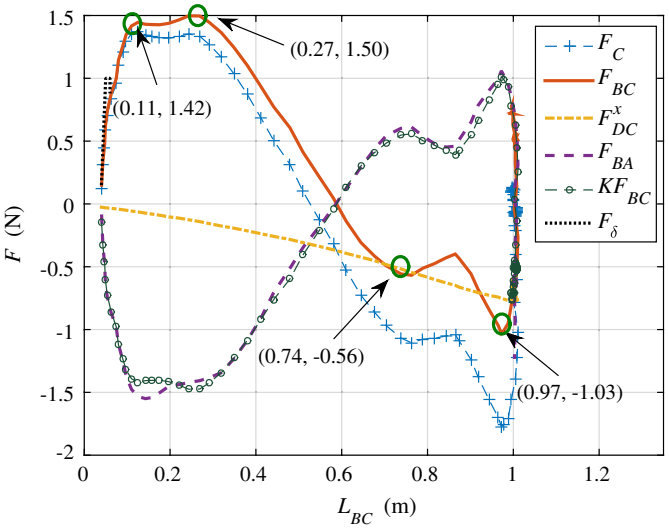

Fig. 11. Deployment forces of the boom in Experiment 1 with focus on the relationship between F_{BA} and KF_{BC}

Fig. 11 shows F^x_{DC}, F_{BC}, F_{BA}, and F_C, the total force acting on the right tip. The initial force F_{BA} was negative because the left tip was deployed in the negative x-direction. The deployment force F_{BC} was calculated by subtracting the GOLS effect force F^x_{DC} from F_C. However, F_{BC} still included the energy relaxation effect of tape springs, friction, and damping. The horizontal force component F^x_{DC} from the GOLS had a small effect on F_C in the beginning of deployment, but increased as the deployed lengths of the booms increased (Fig. 11).

In the beginning F_{BC} increased to a maximum magnitude $F^{\max}_{BC} \approx 1.5$ N at $L_{BC} \approx 0.27$ m (Fig. 11), but decreased quickly due to friction, viscoelastic energy relaxation, and the horizontal force components from the GOLS. For $L_{BC} \geq 0.6$ m, the deployment force F_{BC} was negative due to energy relaxation and friction. It was assumed that the deployment force from the tape springs was equal to zero near the end of deployment ($L_{BC} = 0.97$ m), so the friction force at that time was more than 1 N. Experiment 1 (Fig. 11)

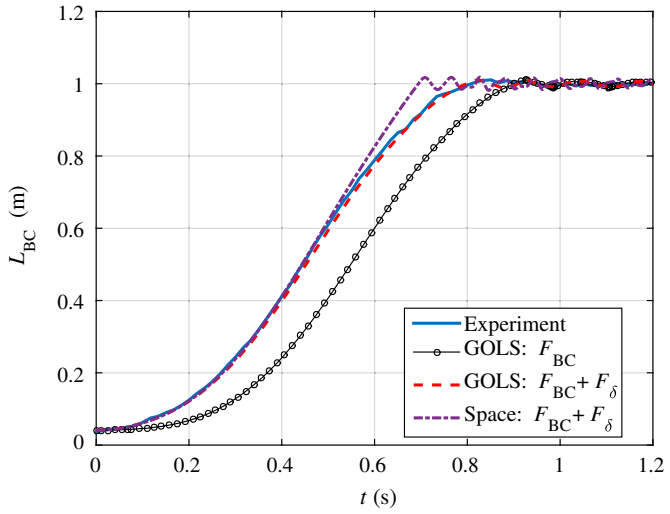

Fig. 12. Deployment length L_{BC} in Experiment 1 and simulations

also showed that $F_{BA} \approx KF_{BC}$ as predicted by Eq. (11). The small deviation between F_{BA} and KF_{BC} was mainly caused by the difference between $\dot{\theta}_A$ and $\dot{\theta}_C$. Since the deviation was acceptably small, $F_{BA} = KF_{BC}$ was used in simulations.

Fig. 12 shows that when F_{BC} (calculated from Experiment 1) was used to simulate the deployment, the booms deployed a little slower than in Experiment 1. The main reason was that an initial kick force existed when the booms started to deploy (Fig. 13). The friction at the very short initial distance was smaller when the tape spring of the last coil was not completely coiled to the spool in the beginning because no contact friction existed between the end of the arcs and coiled tape springs [Fig. 13(a)]. The deployment force from these initial arcs worked as a kick force [Figs. 13(a and b)]. The friction increased when the arc became straight and the spool started to rotate [Fig. 13(c)]. Therefore, an initial kick force was added to the first deployed 20 mm [Figs. 13(a–c)] in simulations.

Fig. 9 shows that the maximum displacement in the y-direction was reached at approximately 0.68 s and decreased after that; therefore, a damping factor, found to be $d_i = 0.2$ Ns/m by comparison of simulation and experiment results, was used in Eq. (13) when $|\theta_i| = \theta_i^{\max}$ to get a similar y-displacement after $\theta_i^{\max}$ was reached (Fig. 14). By similar simulation-experiment comparisons a stiffness factor $\eta_i = 0.001$ was added to satisfy that the maximum acceleration of the hub in the simulation was the same as in Experiment 1 ($a_B = 15$ g). The kick force $F_{\delta} = 1$ N was also added to get a similar deployment time for simulations and Experiment 1 (Fig. 12). A good agreement between displacements in Experiment 1 and in simulation is shown (Fig. 14).

If one assumes that the booms were deployed in space without gravity and the deployment force of the right boom was $F_{BC} + F_{\delta}$,

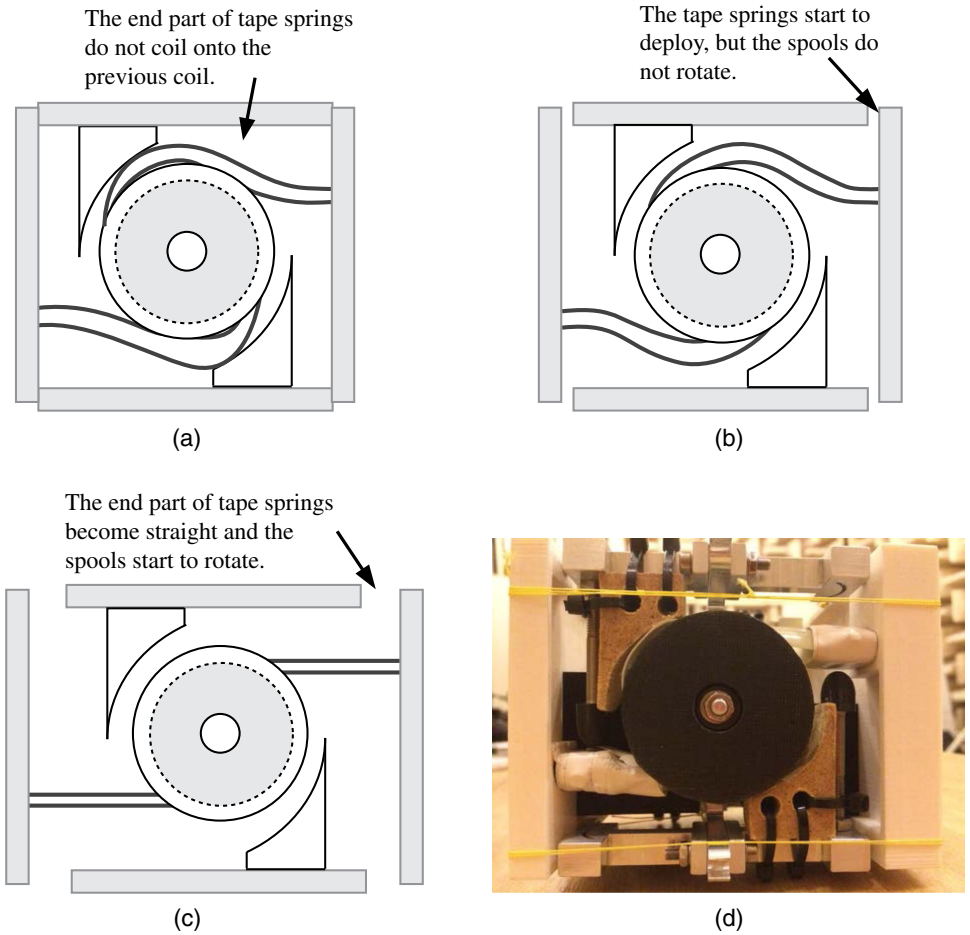

Fig. 13. Initial kick force in the beginning of deployment: (a) the initial stowed configuration of tape springs rolled on a spool with small arc-shaped ends; (b) tape springs start to deploy and generate a kick force; (c) arc-shaped ends become straight; (d) the initial stowed prototype booms assembly (image by Huina Mao)

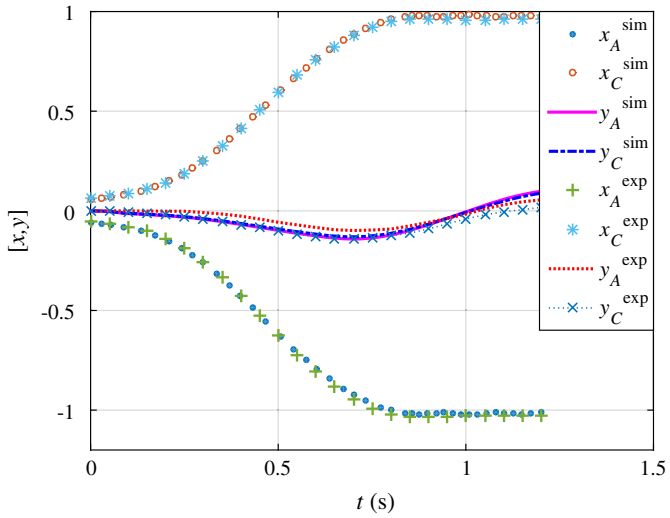

Fig. 14. Better agreement between displacements in Experiment 1 and in simulation when $F_{BC}^{sim} = F_{BC} + F_{\delta}$ is used in simulations

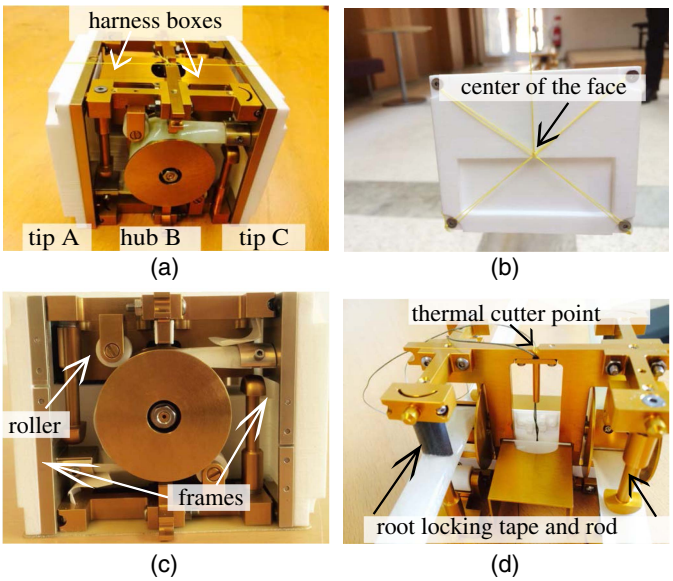

Fig. 15. Engineering qualification model of the self-deployable booms assembly (image by Huina Mao)

the booms would be fully deployed only 0.1 s quicker than in Experiment 1 (Fig. 12). Thus, the effects of the GOLS on the deployment time is small. In space the maximum end-of-deployment shock acceleration of the hub a_B would be approximately 30 g (294 m/s^2) by Eqs. (13)–(16), twice the maximum acceleration in Experiment 1.

Experiment 2: Deployment of the Engineering Qualification Model of the Booms Assembly

Subsequent to Experiment 1 and the prototype booms assembly, an engineering qualification model (EQM) of the booms assembly was fabricated (Fig. 15). The same tape springs were used in both designs, but the EQM had different tip and hub masses, where $m_A = 0.110$ kg, $m_B = 0.4$ kg, and $m_C = 0.115$ kg. To improve the GOLS and the performance of the booms, a new experiment,

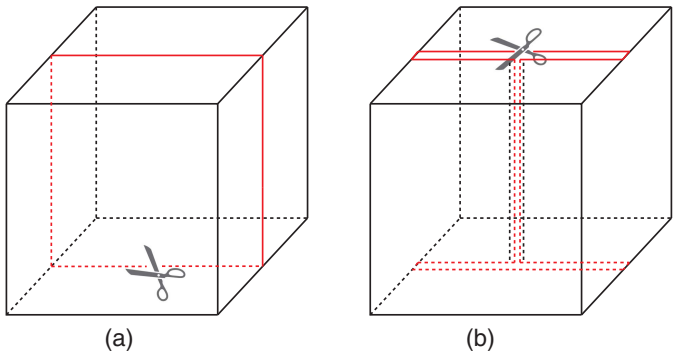

Fig. 16. Route of the constraint UHMW braided cord and cutting points: (a) Experiment 1; (b) Experiment 2

Experiment 2, was performed with an improved GOLS. To further decrease the influence of the GOLS, the EQM was hanging from a much higher ceiling of $h = 15.25$ m. The rotational degree of freedom around the boom axis (x-axis) of the end masses was freed by connecting braided cords to the face center of each tip mass [Fig. 15(b)]. Two new harnesses boxes were added to the hub [Fig. 15(a)]. The harness will be used to transfer information between the center hub and tip sensors and constituted a new source of friction during deployment. Two small rollers were used instead of the arc-shaped wooden pieces to constrain the last coil of the tape springs [Fig. 15(c)]. The rollers aimed to decrease the friction. Two new aluminum frames connected the tape springs with the tip masses [Fig. 15(c)]. A new thermal cutter was designed that would cut the constraining braided cord when the booms were commanded to deploy [Fig. 15(d)]. The constraining braided cord in EQM was not only circled around the outside of the EQM as in the prototype model [Fig. 16(a)], but passed through on the inside of the EQM [Fig. 16(b)].

As for the GOLS in Experiment 1, the EQM booms assembly was hanging from a single point. Since the ceiling was very high in Experiment 2, the maximum angle $\beta_i^{max} = 3.8°$ and the extended length of the extension springs would be less than 33 mm when the booms were fully deployed. Only small length changes of extension springs were needed, so higher stiffness extension springs could be acceptable for Experiment 2, which could also decrease the vertical vibrations in the end. Therefore, in Experiment 2 the booms assembly was hanging only from the braided cords, i.e., without extension springs, and the initial equilibrium state [Fig. 5(a)] was used to decrease the influence of the improved GOLS.

Fig. 17 shows that the booms deployed straighter in x-direction compared to Experiment 1, and that the deployment time was 1.23 s, which was slower than in Experiment 1. The main reason for the longer deployment time was that when the thermal cutter was activated the constraining braided cords had to pass through its route inside the hub to free the tips, which became free at 0.68 s where $L_{BC} = 0.1$ m.

The deployment force of the right boom F_{BC} and the spring force in x-direction F_{Di}^x were calculated from Eqs. (4)–(13) as in Section 4. Thanks to the higher ceiling the maximum influence of the modified GOLS F_{Di}^x was only 0.07 N, i.e., only one-tenth of the influence of the GOLS in Experiment 1 (0.77 N). When the tips had deployed by approximately 0.6 m the deployment force F_{BC} decreased to zero due to viscoelastic relaxation and friction effects (Fig. 18). After $F_{BC} = 0$, F_{BC} became negative, thus the deployment was slowing down. When trying to deploy the booms on a table the friction between the table and end masses was large

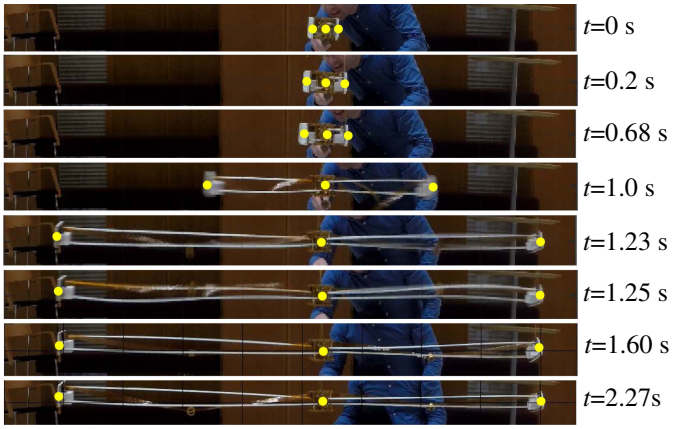

Fig. 17. Snapshots of the deployment sequence of Experiment 2 with the improved GOLS (image by Huina Mao)

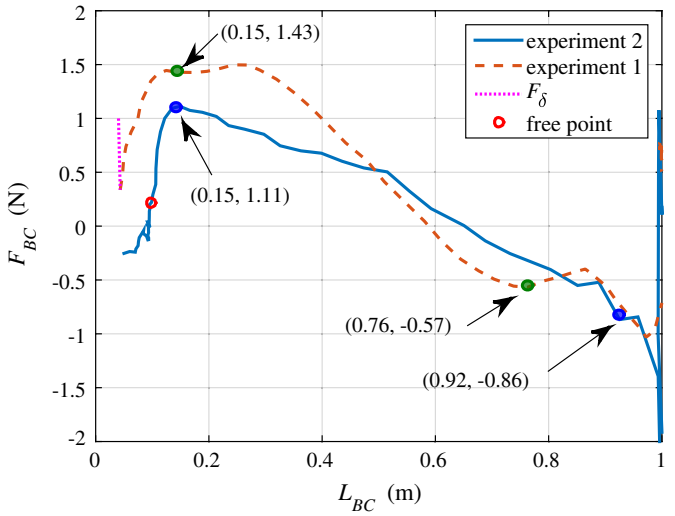

Fig. 18. Experimental deployment force F_{BC}, and the added kick force F_δ for simulation of Experiment 1

enough to prevent full deployment. Assuming that the strain energy in the end of deployment was zero and the deceleration forces from the GOLS were removed, the friction in Experiment 2 would thus be more than 1.4 N at $L_{BC} = 0.99$ m (Fig. 18), compared to approximately 1.0 N in Experiment 1. This might explain that why the maximum deployment force $F_{BC}^{\max}$ was a little smaller in Experiment 2 than in Experiment 1. The strain-energy loss in Experiment 2 was less than in Experiment 1 during deployment when 0.15 m $< L_{BC} <$ 0.76 m (Fig. 18) as the EQM was stowed for only one day at room temperature, compared to the prototype models' stowage time of four months. The tape springs recovered their strain energy after the deployment of Experiment 1 as previously shown by Kwok and Pellegrino (2013).

Fig. 19 shows the simulation results of the EQM in the improved GOLS and without GOLS, i.e., in space conditions. The booms started to deploy at the free point $L_{BC} = 0.1$ m in simulations. The simulation results match those in Experiment 2 when the deployment force of the right tip mass was F_{BC} where F_δ was not included from the free point deployment.

Microcracks had been formed at several places in the 90° direction of the tape springs after repeated coiling and deployment.

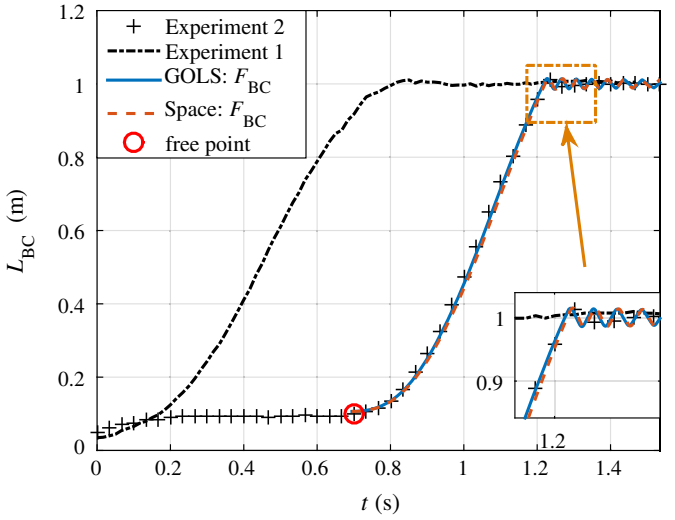

Fig. 19. Deployment length of the right boom L_{BC} in Experiment 1 and 2

Although the microcracks do not cause complete failure of the tape springs, their presence can cause stiffness degradation under both tensile and shear loading (Nairn 1989). The microcracks contribute to a lower strain energy, thus influencing the deployment force and time.

Discussion

Through the simulations and experiments the influence of the GOLS on the deployment force and time was quantified and found to be very small for the improved GOLS of Experiment 2, whereas the effects of friction and viscoelatic strain energy relaxation were significant. In terms of friction effects Jeon and Murphey (2011) found that the measured steady deployment force of the SIMPLE boom is only one-fifth of the ideal force calculated by theory and that the internal friction losses from the deployment mechanism is substantial compared to the released strain energy. In the authors' experiments the deployment forces were calculated after a long time of stowage, so the effects of viscoelastic energy relaxation were also significant.

Theoretical Deployment Force of the Tape Spring Booms

The deployable booms assembly included four bistable tape springs. When the curvature changes from a coiled to an uncoiled stat, the theoretical release of bending energy per length unit is (Iqbal and Pellegrino 2000)

$$\frac{dU_b}{dL} = \frac{1}{2}\beta R\left(\frac{D_{11}}{R_c^2} - \frac{2D_{12}}{R_c R} + \frac{D_{22}}{R^2}\right) \tag{17}$$

with the coiling radius as function of tape spring length (Mallol 2013)

$$R_c = \sqrt{\left(R_{c0} + \frac{h_{\text{tape}}}{2}\right)^2 + \frac{2L_{\text{tape}}h_{\text{tape}}}{\pi}} \tag{18}$$

where the initial coiled radius of the tape spring $R_{c0} = 10$ mm; the length of the coiled part of the tape spring $L_{\text{tape}} = L_{BC}^f - L_{BC}$; the thickness of the tape spring $h_{\text{tape}} = 0.388$ mm; and the

cross section radius of the uncoiled tape spring $R = 7.0$ mm. The approximate **ABD** matrix of the tape spring was calculated by classical laminate theory by dividing each layer into eight plies to tune the bending characteristics without affecting the inplane properties of the material, matrix $\mathbf{B} = 0$ (Prigent et al. 2011; Prigent 2011). The calculated stiffness were $D_{11} = D_{22} = 7.43 \cdot 10^{-2}$ Nm and $D_{12} = 3.36 \cdot 10^{-2}$ Nm.

The total deployment force of four tape springs are $F_{\text{all}} = 4(dU_b/dL) = |F_{AB}| + |F_{BC}|$, where $F_{AB} = KF_{BC}$ and

$$F_{BC} = \frac{1}{1 + |K|} F_{\text{all}} \tag{19}$$

Assume that θ_i is small and changes a little in the deployment, thus from Eq. (12)

$$K = -m_1(m_2 + 2m_3)/[m_3(2m_1 + m_2)] \tag{20}$$

The theoretical deployment force F_{BC} was calculated from Eqs. (17)–(20) and was found to be between 26.8 N and 28.7 N (assuming no friction, damping, microcracks, and viscoelastic relaxation). The theoretical F_{BC} was more than 16 times that of the maximum one in Experiment 1 (1.5 N) and Experiment 2 (1.1 N). Similar discrepancies between deployment times of experiments and simulations with no friction and viscoelastic effects were previously observed (Mallol 2013; Mallol and Tibert 2013).

Since the coiling radius of the two 1-m long tape spring booms varied from 18.8 to 10 mm during deployment, the amplitude of the shear strains in the ±45° layers varied between 1.5 and 0.8% from the smaller to the largest radius. As the shear modulus in ±45° layers of the tape spring decreased during long-term stowage (Murphey and Pellegrino 2004), larger shear strains led to a larger reduction of the shear modulus through viscoelastic relaxations and lower stored energy, i.e., available deployment force. This behavior partly explained why the deployment force in Fig. 18 decreased during the deployment, why the tape springs that had been stored for 10 months only deployed to 90% of their lengths, and why some of the newly manufactured tape springs that were not bistable after fabrication became bistable after being coiled for only a few hours. Manufacturing imperfections, e.g., a small change in tape spring thickness, can lead to large changes in bending stiffness (Peterson and Murphey 2013), and microcracks can cause stiffness losses (Nairn 1989). Hence, it was not possible to separate the effects of viscoelastic relaxation, friction, imperfections and other effects affecting the deployment force.

Conclusion

The presented SEAM booms assembly was based on the patented SIMPLE boom design [Murphey et al. 2010; T. W. Murphey et al., "Deployable space boom using bi-stable tape spring mechanism," U.S. Patent No. 8, 770, 522 (2014)]. The booms were made from four one-meter bistable tape springs coiled on two counter rotating spools and could self-deploy simultaneously from the coiled to the uncoiled configuration. The bistable tape springs were made by four layers of woven glass fibers. The two outside layers (±45°) were used to produce the bistable property and the two inside layers (0°/90°) were used to overcome the viscoelastic relaxation problem to guarantee deployment after long-term stowage. No twist was observed on the cured tape spring because of the approximate symmetric property of the plain-weave fabrics used in fabrication.

One-point GOLS were selected for ground deployment experiments instead of multiple hanging points to allow full free three-dimensional motion. The prototype booms were successfully deployed after being stored for four months at room temperature. Friction and viscoelastic energy relaxation played important roles in the deployment by deceleration of the deployment speed and reduction of the end-of-deployment shock. Viscoelastic strain energy relaxation was a function of the coiled radius and stowage time. A point where the deployment force was zero was found during the deployment, which indicated that the self-deployable property of the tape springs was partially lost as opposing forces from the GOLS and friction effects were balancing the available deployment force. However, the deployment speed at that point was still large enough to fully deploy the booms. Comparison of the deployment forces in experiments and those according to theory showed that the actual deployment force was less than 7% of the theoretical value due to energy relaxation and friction in experiments.

A simple analytical model was presented to predict the deployment of the tape spring booms. The energy relaxation effects were included in the model. The relationship between the deployment forces of the left and right booms were formulated in the model and found through experiments. An initial kick force was added in simulation of the prototype deployment due to the small arc-shaped ends and no contact friction between the arcs and rest of the tape springs. Combined with ground experiments, the analytical model can be used to predict the deployment dynamics of other similar booms in space as the influence of the GOLS can be assessed.

The present study has shown that a simple analytical model can be used effectively to investigate the experimental deployment dynamics of self-deployable tape spring booms and to assess the effects of the gravity offloading system and the combined effects of friction and viscoelastic relaxation.

Acknowledgments

The research is funded by the European Union Seventh Framework Program under grant agreement no 607197. The authors thank Jakob Ekelöw for design and manufacturing of the bistable tape springs and Anton Shipsha and Robert Jansson for improving the manufacturing process. Authors also would like to acknowledge researcher Dr. Ulf Carlsson for his help with the deployment experiments. Special thanks go to Dr. Thomas W. Murphey for the valuable comments on the design of KTH's bistable tape spring booms.

References

Adams, D., and Mobrem, M. (2009). "Lenticular jointed antenna deployment anomaly and resolution onboard the Mars express spacecraft." *J. Spacecr. Rockets*, 46(2), 403–410.

Brinkmeyer, A., Pellegrino, S., and Weaver, P. M. (2016). "Effects of long-term stowage on the deployment of bistable tape springs." *J. Appl. Mech.*, 83(1), 011008.

Brinkmeyer, A., Pellegrino, S., Weaver, P. M., and Santer, M. (2013). "Effects of viscoelasticity on the deployment of bistable tape springs." *19th Int. Conf. on Composite Materials*, International Committee on Composite Materials, Montréal.

Costantine, J., Tawk, Y., Christodoulou, C. G., Banik, J., and Lane, S. (2012). "CubeSat deployable antenna using bistable composite tape-springs." *IEEE Antennas Wireless Propag. Lett.*, 11, 285–288.

Ekelöw, J. (2014). "Design and manufacturing of thin composite tape springs." M.S. thesis, KTH Royal Institute of Technology, Stockholm, Sweden.

Fernandez, J. M., Lappas, V. J., and Daton-Lovett, A. J. (2011). "Completely stripped solar sail concept using bistable reeled composite booms." *Acta Astronaut.*, 69(1–2), 78–85.

Footdale, J. N., and Murphey, T. W. (2011). "Structural design of a CubeSat-based diffractive optic telescope." *52nd AIAA/ASME/ASCE/AHS/ASC Structures, Structural Dynamics and Materials Conf.*, American Institute of Aeronautics and Astronautics, Reston, VA.

Footdale, J. N., and Murphey, T. W. (2014). "Mechanism design and testing of a self-deploying structure using flexible composite tape springs." *42nd Aerospace Mechanisms Symp.*, NASA Goddard Space Flight Center, Greenbelt, MD, 497–510.

Footdale, J. N., Murphey, T. W., and Peterson, M. (2013). "Design and testing of self-deploying membrane optic support structure using rollable composite tape springs." *54th AIAA/ASME/ASCE/AHS/ASC Structures, Structural Dynamics, and Materials Conf.*, American Institute of Aeronautics and Astronautics, Reston, VA.

Greschik, G., and Belvin, W. K. (2007). "High-fidelity gravity offloading system for free-free vibration testing." *J. Spacecr. Rockets*, 44(1), 132–142.

Guest, S., and Pellegrino, S. (2006). "Analytical models for bistable cylindrical shells." *Proc. R. Soc. A*, 462(2067), 839–854.

Heidt, H., Puig-Suari, J., Moore, A., Nakasuka, S., and Twiggs, R. (2000). "CubeSat: A new generation of picosatellite for education and industry low-cost space experimentation." *Proc., 14th Annual/USU Conf. on Small Satellites*, Utah State Univ., Logan, UT.

Herlem, F. (2014). "Modelling and manufacturing of a composite bistable boom for small satellites." M.S. thesis, KTH Royal Institute of Technology, Stockholm, Sweden.

Hexcel Corporation. (2013). "Hexply prepreg technology." ⟨http://www.hexcel.com/Resources/DataSheets/Brochure-Data-Sheets/Prepreg_Technology.pdf⟩ (Jun. 1, 2016).

Hexcel Corporation. (2014). "Hexply M77 product data sheet." ⟨http://www.hexcel.com/Resources/DataSheets/Prepreg-Data-Sheets/M77_eu.pdf⟩ (Jun. 1, 2016).

Iqbal, K., and Pellegrino, S. (2000). "Bistable composite shells." *41st AIAA/ASME/ASCE/AHS/ASC Structures, Structural Dynamics, and Materials Conf. and Exhibit*, American Institute of Aeronautics and Astronautics, Reston, VA.

Ivchenko, N. (2012). "Project proposal to the European Union Framework 7 Program topic SPA.2013.3.1-01: SME space technology research and technology transfer." Small Explorer for Advanced Missions (SEAM), Stockholm, Sweden.

Jeon, S. K., and Murphey, T. W. (2011). "Design and analysis of a meter-class CubeSat boom with a motor-less deployment by bi-stable tape springs." *52nd AIAA/ASME/ASCE/AHS/ASC Structures, Structural Dynamics and Materials Conf.*, American Institute of Aeronautics and Astronautics, Reston, VA.

Kwok, K., and Pellegrino, S. (2010). "Shape recovery of viscoelastic deployable structures." *51st AIAA/ASME/ASCE/AHS/ASC Structures, Structural Dynamics and Materials Conf.*, American Institute of Aeronautics and Astronautics, Reston, VA.

Kwok, K., and Pellegrino, S. (2011). "Viscoelastic effects in tape-springs." *52nd AIAA/ASME/ASCE/AHS/ASC Structures, Structural Dynamics and Material Conf.*, American Institute of Aeronautics and Astronautics, Reston, VA.

Kwok, K., and Pellegrino, S. (2012). "Micromechanical modeling of deployment and shape recovery of thin-walled viscoelastic composite space structures." *53rd AIAA/ASME/ASCE/AHS/ASC Structures, Structural Dynamics and Materials Conf.*, American Institute of Aeronautics and Astronautics, Reston, VA.

Kwok, K., and Pellegrino, S. (2013). "Folding, stowage, and deployment of viscoelastic tape springs." *AIAA J.*, 51(8), 1908–1918.

Lichodziejewski, D., Derbes, B., Slade, K., and Mann, T. (2005). "Vacuum deployment and testing of a 4-quadrant scalable inflatable rigidizable solar sail system." *41st AIAA/ASME/SAE/ASEE Joint Propulsion Conf. and Exhibit*, American Institute of Aeronautics and Astronautics, Reston, VA.

Mallikarachchi, H. M. Y. C. (2011). "Thin-walled composite deployable booms with tape-spring hinges." Ph.D. thesis, Univ. of Cambridge, Cambridge, U.K.

Mallikarachchi, H. M. Y. C., and Pellegrino, S. (2014). "Deployment dynamics of ultrathin composite booms with tape-spring hinges." *J. Spacecr. Rockets*, 51(2), 604–613.

Mallol, P. (2013). "Deployment simulations of a composite boom for small satellites." Licentiate thesis, KTH Royal Institute of Technology, Stockholm, Sweden.

Mallol, P., and Tibert, G. (2013). "Deployment modeling and experimental testing of a bi-stable composite boom for small satellites." *54th AIAA/ASME/ASCE/AHS/ASC Structures, Structural Dynamics, and Materials Conf.*, American Institute of Aeronautics and Astronautics, Reston, VA.

Mobrem, M., and Adams, D. (2009). "Deployment analysis of the lenticular jointed antennas onboard the mars express spacecraft." *J. Spacecr. Rockets*, 46(2), 394–402.

Murphey, T. W., et al. (2015). "High strain composites." *2nd AIAA Spacecraft Structures Conf.*, AIAA SciTech, American Institute of Aeronautics and Astronautics, Reston, VA.

Murphey, T. W., Jeon, S., Biskner, A., and Sanford, G. (2010). "Deployable booms and antennas using bi-stable tape-springs." *24th Annual AIAA/USU Conf. on Small Satellites*, Utah State Univ., Logan, UT.

Murphey, T. W., and Pellegrino, S. (2004). "A novel actuated composite tape-spring for deployable structures." *45th AIAA/ASME/ASCE/AHS/ASC Structures, Structural Dynamics, and Materials Conf.*, American Institute of Aeronautics and Astronautics, Reston, VA.

Nairn, J. A. (1989). "The strain energy release rate of composite microcracking: A variational approach." *J. Compos. Mater.*, 23(11), 1106–1129.

Peterson, M. E., and Murphey, T. W. (2013). "Large deformation bending of thin composite tape spring laminates." *54th AIAA/ASME/ASCE/AHS/ASC Structures, Structural Dynamics, and Materials Conf.*, American Institute of Aeronautics and Astronautics, Reston, VA.

Prigent, Y. (2011). "A finite model of bi-stable woven composite tape-springs." M.S. thesis, KTH Royal Institute of Technology, Stockholm, Sweden.

Prigent, Y., Mallol, P., and Tibert, G. (2011). "A classical lamination model of bistable woven composite tape-springs." *24th Nordic Seminar on Computational Mechanics (NSCM)*, Dept. of Civil and Structural Engineering, Aalto Univ., Espoo, Finland, 51–54.

Reveles, J., Lawton, M., Fraux, V., and Gurusamy, V. (2015). "The development of a low mass extendible composite boom for small satellite applications." *29th Annual AIAA/USU Conf. on Small Satellites*, AIAA, Reston, VA.

Tsuda, Y., et al. (2011). "Flight status of IKAROS deep space solar sail demonstrator." *Acta Astronaut.*, 69(9–10), 833–840.